Preference of cluster isomers as a result of quantum delocalization: Potential energy surfaces and intermolecular vibrational states of Ne$\cdots$HBr, Ne$\cdots$HI, and HI(Ar)$_n$(n=1-6)

Petr Slavíček, Martina Roeselová, and Pavel Jungwirth *

J. Heyrovský Institute of Physical Chemistry, Academy of Sciences of the Czech Republic and Center for Complex Molecular Systems and Biomolecules, Dolejškova 3, 18223 Prague 8, Czech Republic

Burkhard Schmidt

Freie Universität Berlin, Department of Mathematics/ Scientific Computing, Arnimallee 2-6, 14195 Berlin, Germany

Abstract

Intermolecular vibrational states are calculated for Ne$\cdots$HBr, Ne$\cdots$HI, and HI(Ar)$_n$ (n=1-6) complexes using potential energy surfaces constructed by accurate *ab initio* methods. Potentials of rare gas–hydrogen halide clusters exhibit two collinear minima, one corresponding to hydrogen lying between the heavy atoms, and the other to hydrogen facing away from the rare gas atom. The relative depths of the two minima are a result of a subtle balance between polarization and dispersion interactions. Moreover, due to a large quantum delocalization in the hydrogen bending (librational) motion the relevance of a particular stationary point on the potential energy surface is only limited. It is more appropriate to discuss the isomers in terms of vibra-

*Author to whom correspondence should be addressed.

Electronic mail: jungwirt@jh-inst.cas.cz.

tionally averaged structures. For Ne$\cdots$HBr the potential minimum and the vibrationally averaged structure correspond to the same isomer with hydrogen between neon and bromide. However, for Ne$\cdots$HI the global minimum corresponds to the Ne–IH collinear geometry, while the vibrationally averaged structure has hydrogen between the heavy atoms. In the case of HI(Ar)$_n$ we show that one can flip between the two isomers by adding argon atoms, which reconciles the seemingly contradictory experimental results obtained for the photodissociation of HI$\cdots$Ar on one side, and of large HI(Ar)$_n$ clusters on the other side.

I. INTRODUCTION

Small hydrogen halide–rare gas clusters serve as prototypes of mixed weakly bound systems for studying intermolecular interactions. Considerable attention has been paid, both by theory and experiment, to the structure and interactions of systems with a single rare gas atom, i.e. of Rg$\cdots$HX complexes, where Rg is most often neon or argon, and X=F, Cl, Br, or I [1–15]. In all cases, the potential energy surface (PES) of the complex exhibits two distinct minima, one corresponding to the Rg–HX and the other to the Rg–XH isomer, separated by a relatively shallow barrier [7–12]. The former structure, where the hydrogen lies between the heavy atoms, is stabilized primarily by polarization forces, since in this geometry the permanent dipole and quadrupole of the HX moiety induces an attractive electric response of the rare gas atom. On the other hand, for the latter isomer, where hydrogen points away from the rare gas atom, dispersion interaction between the heavy atoms dominates. This simple qualitative analysis allows to rationalize the fact, that hydrogen fluoride and chloride with a large ionic character prefer the Rg–HX isomer, while for hydrogen bromide and especially iodide, which are more covalently bound, dispersion interactions are competitive enough, so that in some cases the Rg–XH structure actually becomes more stable.

The knowledge of the structure of Rg$\cdots$HX complexes is not only interesting *per se* but it is also important in connection with the cage effect [16] in clusters. The cage effect, which is the ability of the environment to hinder the photodissociating solute molecule, has been investigated in great detail in hydrogen halide–rare gas clusters [17–30]. Although a single Rg atom is rather inefficient in hindering the photolyzed highly energetic hydrogen, in larger rare gas clusters caging becomes much more important. It has been shown recently, that the efficiency of caging depends not only on the cluster size, but also on the position of the HX impurity (embedded vs. surface), and, especially for the surface structures, on the particular initial orientation of the hydrogen atom [25,30].

A necessary condition for understanding the vibrational dynamics and for interpreting the spectra of the Rg$\cdots$HX complexes is a construction of an accurate PES. This is achieved either by inverting experimental data obtained by high resolution vibrational/rotational spectroscopy, or by state-of-the-art quantum chemical calculations. Recently, attempts have been made to merge the two approaches, and a pre-calculated PES has been improved via a "morphing" procedure using spectroscopic data [5]. Currently, high quality potentials exist for Ar$\cdots$HF, Ar$\cdots$HCl, Ar$\cdots$HBr, Ar$\cdots$HI, and Ne$\cdots$HCl complexes [5,7–12]. In this paper, we provide hitherto uninvestigated PESs of the Ne$\cdots$HBr and Ne$\cdots$HI complexes, important for the interpretation of recent photodissociation cluster experiments [31,32].

An interesting feature of hydrogen halide–rare gas clusters is connected with the fact that they are typically prepared via supersonic expansion into the vacuum through a narrow nozzle [33]. This technique leads to a very efficient cooling of the nascent clusters to temperatures ranging between several and several tens of Kelvins. Under these cryogenic conditions quantum vibrational effects cannot be neglected. This is particularly true for the cold and light hydrogen atom, which moves in a shallow intermolecular bending potential exhibiting a large amplitude bending (librational) motion [7,34]. Due to this librational hydrogen delocalization, and partly also due to the soft intermolecular stretch (which actually couples to a certain extent with the hydrogen bend) the physical relevance of a particular point, minimum or saddle, on the PES of a Rg$\cdots$HX complex is strongly limited. One should rather think in terms of vibrationally averaged structures, where the quantum effect of delocalization due to zero point motions is properly taken into account. In the present study, we demonstrate this issue on several examples, including an extreme case, where the vibrationally averaged structure corresponds to an isomer different from the global minimum on the PES. In thisconnection note that the flip of isomers upon inclusion of zero point energy is not limited to Rg$\cdots$HX systems. As has been shown recently, this effect is also found e.g., for the energetically lowest isomers of water hexamer [35]. In addition we demonstrate, that in the case of HI(Ar)$_n$ (n=1-6) one can actually flip between the isomer with the hydrogen pointing away from the cluster and that with hydrogen between the heavy atoms by simply adding argon atoms. We show that this finding reconciles seemingly contradictory experimental results on small vs. large clusters. [31,32,36].

The rest of the paper is organized as follows. System and geometry are briefly described in Section II, and Section III provides the computational details. Results and discussion are presented in Section IV. Finally, Section V contains concluding remarks.

II. SYSTEMS AND GEOMETRY

In this paper, we present *ab initio* potential energy surfaces and calculations of intermolecular vibrational states of Ne$\cdots$HI and Ne$\cdots$HBr van der Waals complexes. Librational calculations have also been performed for $\mathrm{HI(Ar)}_n$ (n=1–6) clusters. For the calculation of vibrational states of Rg$\cdots$HX clusters we used the standard Jacobi coordinates. R is the distance between the rare gas atom and center of mass of hydrogen halide molecule, r is the internuclear distance for the HX molecule and Θ is the angle between vectors $\vec{R}$ and $\vec{r}$. These coordinates are depicted on Fig. 1. For the *ab initio* calculations we used slightly different coordinates, with R being the distance between the halogen atom and the rare gas atom. Since the centers of mass of both HBr and HI practically coincide with the halogen atoms, for all practical purposes the difference between the two coordinate sets can be neglected. Finally, the black dot in Fig. 1 marks the localization of the bonding basis functions (see next section).

III. COMPUTATIONAL DETAILS

A. *Ab initio* method

It is well known that for the Rg$\cdots$HX complexes the dispersion energy is an important part of interaction energy. Therefore, for an adequate description of such systems it is imperative to include a dominant part of electron correlation. In the calculations reported here, we have used coupled clusters CCSD(T) method and for comparison also the second order Møller-Plesset perturbation theory (MP2). Due to their size extensivity both MP2 and CCSD(T) methods are appropriate for intermolecular energy calculations.

We have calculated the intermolecular energy within the supermolecular approach, in which the interaction energy is given as a difference between the total energy of the complex (E_{RgHX}) and the sum of the energies of the subsystems (E_{HX} + E_{Rg}). Within this approach, removal of basis set superposition error (BSSE) is absolutely necessary. We have, therefore, applied the standard counterpoise method (CP) [37], including both atom centered and bond basis functions.

The quality of intermolecular energy calculations for weakly bound systems strongly depends on the choice of the electronic basis. The employed basis set, presented in detail in Table I, has an atom centered and bond region centered parts. The latter part is common for all complexes under investigation. The atom centered basis functions for H, Ar, Br and Cl correspond to the aug-cc-pVDZ basis set [38]. These standard basis sets have been augmented by one function of d symmetry (for hydrogen), or of f symmetry (for chlorine, argon and bromine), with exponents of 0.15 (H), 0.23 (Ar), 0.15 (Cl) and 0.25 (Br) [39–43]. All these exponents were optimized with respect to the dispersion term [43]. For neon we have used the augmented double-ζ ANO basis set [42]. While for Rg$\cdots$HX complexes with X=Cl or Br the calculations include all electrons, for systems with iodine we have used an average relativistic effective potential (AREP) [44]. We have modified the iodine valence double-ζ basis proposed in this work in the same way as described in Refs. [45,46] by adding one polarization d function with an exponent of 0.28 and s and p diffuse functions with exponents of 0.03335 and 0.04536. For Ar$\cdots$HI test calculation we have used also a correlation consistent polarized triple-ζ basis set [45]. This basis set has served originally for relativistic all electron calculation, therefore, we have modified it in a similar way as in Ref. [47]. Namely, we have neglected the core atomic orbitals and we have assumed only the large component basis.

It has been demonstrated in Ref. [48–51] that adding a small number of basis functions to the mid-bond region is a very efficient way for improving the description of dispersion energy.

Whereas the location of such basis functions for atom–atom systems is straightforward [48], the situation for anisotropic systems is more ambiguous. Fortunately, the results are not very sensitive to the exact location of these functions in the intermolecular bond region [50]. We have found that a balanced description is achieved when the bonding functions are placed in the middle of the abscissa given by midpoints of Rg–X and Rg–H bonds (see Fig.1). This bond basis consists of the three s functions (exponents of 0.9, 0.3 and 0.1), three p functions (exponents of 0.9, 0.3 and 0.1) and two d functions (exponents of 0.6 and 0.2). This set has been successfully applied to rare gas dimers [48] and to various anisotropic systems, such as Ar$\cdots$HF, Ar$\cdots H_2O$ and Ar$\cdots NH_3$ [49]. According to these studies, the interaction energies are rather insensitive to the change of the orbital exponents and the set should be broadly applicable to different intermolecular systems.

All *ab initio* calculations reported in this paper have been performed using the GAUSSIAN 98 program package [52].

B. Calculation of vibrational states

The bound states of Ne$\cdots$HBr and Ne$\cdots$HI complexes were calculated using the coupled channel scheme in which the total wavefunction is expanded in terms of rotational functions of the HX molecule. We used an exact Hamiltonian for an atom – (rigid) diatom system expressed in standard Jacobi coordinates (see Fig. 1)

$$\hat{H} = -\frac{\hbar^2}{2\mu_1}\left(\frac{1}{R}\frac{\partial^2}{\partial R^2}R - \frac{\hat{l}^2}{\hbar^2 R^2}\right)+\frac{\hat{j}^2}{2\mu_2 r^2} + V(R,\Theta) \tag{1}$$

where $\mu_1 = \mathrm{M}_{Rg}\mathrm{M}_{HX}/(\mathrm{M}_{Rg} + \mathrm{M}_{HX})$ is the reduced mass of the Rg$\cdots$HX complex, μ_2 is the reduced mass of the HX molecule, $\hat{l}$ is the angular momentum operator for end-over-end rotation of the complex (i.e. corresponding to the R coordinate), and $\hat{j}$ is the angular momentum of the internal rotation of HX, which is assumed to be a rigid rotor with the internuclear distance r fixed to its equilibrium value. Finally, $V(R,\Theta)$ is the intermolecular potential for interaction of a HX molecule with a rare gas atom.

In this study, we have assumed that the total angular momentum $\hat{J} = \hat{j} + \hat{l}$ is equal to zero. This leads to a significant reduction of the number of coupled states (and thus the number of the coupled equations to be solved), and also to simplification of the Hamiltonian since then $\hat{l}^2 = \hat{j}^2$. The total wave function can be then expanded in spherical harmonics $Y_{j0}(\Theta)$ of the $C_{\infty v}$ point group describing the angular degrees of freedom corresponding to the internal rotation of the HX molecule

$$\Psi(R,\Theta) = \frac{1}{R}\sum \chi_{j0}(R)Y_{j0}(\Theta) \tag{2}$$

Substitution of the above expansion into the total Schrödinger equation with the Hamiltonian given by Eq.(1) yields a set of coupled equations for the radial functions $\chi_{jm}(R,t)$:

$$\begin{aligned} i\hbar\frac{\partial}{\partial t}\chi_{j0}(R,t) = &\Big[-\frac{\hbar^2}{2\mu_1}\frac{\partial^2}{\partial R^2} + \Big(\frac{\hbar^2}{2\mu_1 R^2} + \frac{\hbar^2}{2\mu_2 r^2}\Big)j(j+1)\Big]\chi_{j0}(R,t) \\ &+ \sum_{j'} \chi_{j'}(R,t)V_{jj'} \end{aligned} \tag{3}$$

where the potential matrix is defined by $V_{jj'} = \langle j'0|V(R,\Theta)|j0\rangle$. The radial wavefunction is represented on a spatial grid of 256 equidistant points. We solved this set of equations using the imaginary time propagation scheme [53], where Chebyschev propagator with a timestep of $\tau = 25$ fs was employed. We truncated the expansion into spherical harmonics at $j_{max} = 7$, which leads to fully converged results. Typically, 100 timesteps are required to fulfill the criterium $\langle\Psi(t+\tau)|\Psi(t)\rangle > 1 - 1\times 10^{-7}$. Vibrationally excited states were also obtained by imaginary time propagation, where at each evaluation of the Hamiltonian the contribution of lower states is projected out. For the systems under study, all bound states can be reliably obtained in this way [53].

For the construction of vibrational states of larger clusters with more than one rare gas atom, it is not computationally feasible to perform the calculations in full dimensionality. Therefore, we have used a partially separable approach, analogous to that used in our previous studies [29,30]. Briefly, the total wavefunction is expressed as:

$$\Psi(q_1, q_2, ..., q_{3n-6}, \Theta, \Phi) = \phi_1(q_1)....\phi_{3n-6}(q_{3n-6})\phi_{lib}(\Theta, \Phi, \{q_i\}) \tag{4}$$

where q_i are the normal coordinates of the cage (i.e. heavy atoms). The cage modes are taken into account within the harmonic approximation, while the librational wavefunction of the HX molecule $\phi_{lib}(\Theta, \Phi)$ is calculated by diagonalization of the HX (hindered) rotational Hamiltonian in the basis of spherical harmonics, i.e. we assume only the last two terms on the right hand side of Eq.(1):

$$\hat{H} = \frac{\hat{j}^2}{2\mu_2 r^2} + V(\Theta, \Phi, \{q_i\}) \tag{5}$$

The term connected with the overall rotation of the cluster is neglected since $\mu_1 R^2$ is much larger than $\mu_2 r^2$. Due to the loss of cylindrical symmetry the potential V is in such cases also Φ–dependent. Finally, both the potential for the hindered rotation of HX and the librational wavefunctions are parametrically dependent on the cage coordinates.

This approach is satisfactory for systems, where the minima corresponding to HX–Rg_n and XH–Rg_n structures are well separated or correspond to similar heavy atom geometries and, therefore, we can separate the bending and stretching modes. The energy gap between minima corresponding to possible isomeric structures is increasing with the number of rare gas atoms. As will be discussed in detail in the section IV.B calculations in full dimensionality for the case of the smallest HX-Rg clusters indiactes that the approximate approach is reasonable, in particular for the ground state wavefunction. Thus, the coupling between vibration and internal rotation does not have a strong effect on the ground state structure of the explored complexes (Ar$\cdots$HI and Ne$\cdots$HI), however it can seriously influence the excited bound state.

IV. RESULTS AND DISCUSSION

A. Test calculations

In order to confirm the reliability of the employed *ab initio* method and basis sets, we have performed test calculations on Rg$\cdots$HX systems for which good empirical or semiempirical potential are available. Thus, we have first reinvestigated Ar$\cdots$HCl, Ne$\cdots$HCl, Ar$\cdots$HBr and Ar···HI complexes. We have calculated the interaction energies both at the MP2 and CCSD(T) levels. The results of our calculations are listed in Table 2.

The agreement between experimental potentials and calculated *ab initio* values is strikingly good. For Ar···HCl, the global minimum lies 175 cm^{-1} under the dissociation limit [7], while the calculated value at the CCSD(T) level is –173 cm^{-1}. For the secondary minimum values of –139 cm^{-1} and –141 cm^{-1} are the experimental and calculated dissociation energies. Similarly, the experimental dissociation energies for the global and the secondary minimum of Ar···HBr complex are -165 and -160 cm^{-1} [12], while the present calculations give -168 and -158 cm^{-1}. Also for Ne···HCl cluster our calculations are very close to experimental values [8]: -68 vs. -66 cm^{-1} for the global minimum and -53 vs. -52 cm^{-1} for the secondary minimum. The MP2 interaction energies are close to the CCSD(T) values for Ne···HCl, while MP2 overestimates the binding energy by approximately 20 cm^{-1} for Ar···HBr and Ar···HCl. However, the difference in energies between the global and the secondary minima are very similar for the MP2 and CCSD(T) calculations and for empirical potentials.

For the Ar···HI complex, we have calculated the energy of the global minimum to be -185 cm^{-1} at the CCSD(T) level, while the recently published semiempirical potential gives of –220 cm^{-1}, the values for secondary minimum being -148 and -172.7 cm^{-1}, respectively. The agreement is satisfactory and our calculations reproduce also the shape of the semiempirical potential and provide the correct order of the global and the secondary minima. Note also, that the MP2 energies are shifted by 30 cm^{-1} and are very close to the semiempirical potential (which is actually based on MP2 calculations). We stress already here that the difference between MP2 and CCSD(T) is much smaller for Ne···HI than for the Ar···HBr and Ar···HCl complexes. We have also tested a larger iodine basis set of a triple-ζ quality, yielding the CCSD(T) global and secondary minima of -193 and -149 cm^{-1}, which is very close to the results obtained with the double-ζ quality basis set. Note also that our calculated value of the dissociation energy corrected for zero point vibrations would lie between the value of -93 cm^{-1} given by Heaven [54] on the basis of HI-Ar photodissociation experiment and the value of -146.4 cm^{-1} based on the semiempirical potential of Bevan et al. [5].

B. Potential energy surfaces of Ne$\cdots$HBr and Ne$\cdots$HI

We have calculated *ab initio* interaction energies on an R and Θ grid, constraining the H-X bond distance to its equilibrium value of 1.414 Å for HBr and 1.609 Å for HI. The HX–Rg angle Θ has been varied from 0 to 180^o with a 30^o step and the X-Rg coordinate R has been varied from 3.2 Å to 6.0 Å with a step of 0.1 Å around the minima and 0.5 Å elsewhere. All energies have been calculated at the CCSD(T) level, except for repulsive geometries with highly positive energies, where MP2 energies practically coincide with the CCSD(T) energies and the MP2 description, therefore, suffices. Thus, we have represented the Ne$\cdots$HBr and Ne$\cdots$HI interaction potential by approximately 90 points calculated at the CCSD(T) level.The potential was then interpolated by cubic splines. The Ne$\cdots$HBr PES is depicted in Fig.2, and the Ne$\cdots$HI potential is depicted in Fig.3. These figures have been produced using the CCSD(T) interaction energies, however, MP2 interaction energies are typically only 2-3 cm^{-1} above those obtained using the CCSD(T) method. This correspondence implies that the results are converging well with respect to recovering the correlation energy.

The general features of the Ne$\cdots$HI and Ne$\cdots$HBr PESs are similar to those of analogous Rg$\cdots$HX complexes. Namely, these potential functions are characterized by two minima, and both the global and secondary minima correspond to collinear geometries. Important characteristics of the potentials such as geometries and energies of the global minimum, secondary minimum, and the barrier between them are listed in Table 3. The global minimum of the Ne$\cdots$HBr complex lies 58.6 cm^{-1} below the dissociation limit. The $\Theta = 0^o$ value for this minimum corresponds to neon facing the hydrogen with $R_m = 4.07$ Å . The secondary minimum is energetically very close to the global minimum: energy of –55.7 cm^{-1} at $\Theta =$ 180^o (neon is on the other side of the halogen atom than hydrogen), and R_m =3.55Å. The two minima are practically isoenergetic, however, as will be discussed in the next section the zero point energy clearly prefers the former structure. The transition state between these two minima has an energy of -30.5 cm^{-1} at $\Theta = 90\ ^o$ and $R_m = 4.00$ Å. Another important feature of this PES is its anisotropy. The value of the optimal distance R_m for a given Θ continuously decreases with increasing Θ.

For the Ne$\cdots$HI complex, the global minimum corresponds to neon on the other side of the halogen atom than hydrogen ($\Theta = 180^o$, $R_m = 3.75$ Å). The energy of this point on the potential energy surface is -55.7 cm^{-1}. The secondary minimum (for $\Theta = 0\ ^o$) lies 7.6 cm^{-1} above the global minimum and its corresponding intermolecular distance R is 4.48Å. The transition state is characterized by $R_m = 4.3$ Å and $\Theta = 90\ ^o$ and the height of the barrier is 28.5 cm^{-1}.

As one can see from Figs. 2-3, both for the Ne$\cdots$HBr and Ne$\cdots$HI complexes the binding energy is small and potentials are rather flat. Note, that for such systems one should be careful with identifying the equilibrium structure of the molecular system with the global minimum on the PES. Instead, the concept of vibrationally averaged structures, which takes into account the effect of zero point motions, should be employed.

The shape of the Ne$\cdots$HBr and Ne$\cdots$HI PESs is similar to those of the other members of the homologous series Rg$\cdots$HX (Rg=Ne,Ar; X=F,Cl,Br and I). The quantitative differences can be well understood in terms of the competition between dispersion and polarization interactions. While polarization prefers Rg-HX isomers, dispersion favors the HX-Rg geometries. Therefore, lighter halogens with a larger HX dipole have the former structure as a global minimum, while the latter arrangement is optimal for the Ar$\cdots$IH complex. Finally, the polarizability of neon is much smaller than that of argon, which results in smaller interaction energies.

Quantitatively, taking into account polarization and dispersion interaction, we obtain for the E_{Ne-HX}/E_{Ar-HX} energy ratio the following expression [55]:

$$\frac{E_{Ne-HX}}{E_{Ar-HX}} = \frac{\alpha_{Ne}}{\alpha_{Ar}}\left(\frac{r_{Ar}}{r_{Ne}}\right)^6 \frac{aI'_{Ne} + m}{aI'_{Ar} + m} \tag{6}$$

where $I'_{Rg} = I_{Rg}I_{HX}/(I_{Rg} + I_{HX})$, $a = (2/3)\alpha_{HX}$, and $m = 4\mu^2_{HX}/4\pi\epsilon_0$. I is the ionization potential, μ the dipole moment, and α the polarizability. Taking Ar$\cdots$HBr and Ar$\cdots$HI semiempirical potentials as an existing reference, we obtain the global and secondary minima at –58 and –53 cm^{-1} for Ne$\cdots$HBr and at –62 and –49 cm^{-1} for Ne$\cdots$HI. These estimated numbers are in a good agreement with our calculated *ab initio* interaction energies. We conclude by noting that further improvement of our potentials using the "morphing" approach [10] would be possible when albeit limited experimental information on systems under study becomes available.

C. Bound states

One of the goals of this work is to explore the structure of the Ne$\cdots$HI and Ne$\cdots$HBr complexes in their ground states. With the knowledge of the potential energy surfaces of these complexes one can expect the large amplitude motion of the hydrogen atom to have a significant effect even in the ground state. Therefore, the usual concept of the structure as a geometry corresponding to the minimum on PES could be inadequate.

Vibrational wavefunctions of the bound states of the Ne$\cdots$HI complex are depicted in Figs. 4,5, and 6. Wavefunctions for the Ne$\cdots$HBr cluster look similar, therefore we do not present them here. Figure 4a shows a contour plot of the square of the ground state wavefunction of the Ne$\cdots$HI complex in R and Θ coordinates. Note that because the ground state wavefunctions are of Σ^+ symmetry, there is no Φ dependence. These wavefunctions have maximum at $\Theta = 0^o$ both for Ne$\cdots$HBr and Ne$\cdots$HI. If we adopt the concept of vibrationally averaged structures, then such wavefunctions correspond to hydrogen pointing towards the neon. This is not surprising in the Ne$\cdots$HBr case where this structure is also the minimum on the PES. On the other hand, the minimum on the Ne$\cdots$HI PES corresponds to the Ne–IH collinear structure (i.e. $\Theta = 180^o$). In this case, the structure is determined primarily by the quantum zero point motion connected with the shape of the potential, namely by the large amplitude motion of hydrogen atom in the angular coordinate. The value of the vibrationally corrected binding energy D_0 is -29.0 cm^{-1} for Ne$\cdots$HBr and -28.3

cm^{-1} for Ne$\cdots$HI, the average R being 4.1 Å and 4.3 Å, respectively. For the Ne$\cdots$HI case, this distance is significantly larger than that for the absolute minimum (R=3.75 Å). The wavefunction for Ne$\cdots$HBr is similar in shape (the difference in R is given by different HX bond length for HBr and HI), and very close in energy. Note at this point that the electronic binding energy D_e for the Ne–HBr isomer is -58.6 cm^{-1}, while only -48.1 cm^{-1} for the Ne–HI isomer. However, since the rotational constant B is larger for HBr (8.473 cm^{-1}) [56] than for HI (6.342 cm^{-1}) [5], the differences in potential energy and in the rotational constants partly cancel each other. The discrepancy between geometries corresponding to the global minimum on the PES and to the vibrationally averaged geometry pertains also for the Ne$\cdots$DI complex. The wavefunction (not shown here) is even more localized in the Ne$\cdots$DI bending motion. It is clearly seen from the Fig. 4a that the wavefunction of the ground state is well separable in R amd Θ. This provides further justification of the approximations used for larger clusters based on the bend/stretch separation.

Another interesting question is whether we can change the structure by vibrational excitation, i.e. whether we can identify some of the excited states with the second isomer. We have, therefore, calculated several low-lying bound states of the systems under investigation. The calculated energies of the lowest states are listed in Table 4. It can be generally said that the interpretation of the excited bound states in ithe sense of the second isomer is not straightforward. Figs. 4 and 5 show the squares of the moduli of the wavefunctions of bound states of Σ^+ symmetry. The first state is the above discussed ground state (-28.3 cm^{-1}) corresponding to the Ne–HI structure (Fig. 4a), while Fig.4b depicts an excitation of Ne$\cdots$HI complex with energy -16.1 cm^{-1}, which is the third state of Σ^+ symmetry. This excitation is predominantely of a stretching character which is implied by one node along R coordinate for $\Theta=0^o$. However, certain degree of bending excitation is also clearly present. Fig. 5a then contains the second state of Σ^+ symmetry (-19.4 cm^{-1}). The state has one nodal plane roughly diagonal in (R,Θ) plane. Hence, there is no clear distinction between stretch and bend excitation in this case. However, this wavefunction prefers the neon on the side opposite of the hydrogen with $\Theta = 180^o$ and thus we can basically interpret this state as a Ne–IH isomer. The stretching excitation of this state can be then seen in Fig. 5b (-9.7 cm^{-1}). Again the nodal structure is not simple. This state as well as the previous ones of Σ^+ symmetry are far from being separable in R and Θ. The interpretation of the excited states of Π symmetry is more obvious, see Fig. 6. The lowest state of this symmetry (-12.4 cm^{-1}) is simply an almost free HI rotor state with j = 1 (with $\cos\Phi$ or $\sin\Phi$ dependence) and the corresponding first excited state (-2.3 cm^{-1}) has the same angular dependence but additional stretching excitation in R coordinate. Unlike for the Ar$\cdots$HI complex [5], we can not interpret these T–shaped states with maxima near Θ=90^o as bending excitations of certain isomer, such as Ne–HI or Ne–IH.

It is interesting that also states with positive energies are found by imaginary time propagation. These levels correspond to higher states of Π symmetry with total energy above the dissociation threshold of the weakly bound complex. Because of a weak coupling between radial and angular motions these resonances have very long lifetime and should, therefore, be in principle spectroscopically observable. A lower limit of a few nanoseconds for their lifetime was found by real time propagation using Chebyschev expansion of the time evolution operator [57].

In conclusion of this section, let us briefly summarize possible relations between the minima of the PES and the ground state vibrationally averaged structures. As already noted, complexes of Rg and HX can have two basically collinear structures, either Rg–HX or Rg–XH. Table 5 represents three possible situations which can occur in these weakly bound complexes. The first case is the most typical one where both the global minimum on the PES and the vibrationally averaged structure are found at Θ=0^o (Rg–HX). As typical representative of this family of complexes we have discussed Ne$\cdots$HBr. The only known case where the situation is exactly opposite is the Ar$\cdots$HI complex [5]. The third, hithertho unexplored, possibility is the case with the flip of the hydrogen atom upon including the zero point motion, as has been demonstrated in this work on Ne$\cdots$HI. A general feature of all these complexes is that zero point motion tends to prefer the Rg–HX structure. This allows us to be confident that even though the difference in the energies of the Ne–HBr and Ne–BrH minima might be within the accuracy of the *ab initio* method employed, the structure in any case corresponds to the Ne–HBr arrangement.

D. Larger clusters: flip of the hydrogen wavefunction

As discussed in the previous section, the ground state structures of Ne$\cdots$HBr and Ne$\cdots$HI clusters correspond to hydrogen facing the rare gas atom, despite the fact that the global minimum of Ne$\cdots$HI complex lies at the opposite side. This is in contrast to the ground state structure of Ar$\cdots$HI complex which corresponds to argon facing directly to the halide (i.e. to the Ar–IH arrangement). For this structure, a conclusive experimental evidence has been provided by Wittig et al. [36]. We now address the following question: How does the structure (i.e. the hydrogen wavefunction) change with increasing number of rare gas atoms in the cluster? This is of a particular interest for the interpretation of experiments concerning photodissociation of HX molecule on the surface of rare gas clusters. After the UV photolysis, systems with hydrogen wavefunction localized between halogen and rare gas atoms will be characterized by a strong cage effect resulting in a significant peak at low energies in the final hydrogen kinetic energy distribution (KED) spectrum. On the other hand, if the hydrogen initially faces away from the cluster, the cage effect will be negligible [29,30,58]. In this study we have varied the number of the cage atoms from single argon atom to six argon atoms. The extrapolation to larger clusters is then straightforward, since six argons constitute first solvation half-layer for every larger rare gas cluster with a single substitutional HX impurity on the cluster interface. The interaction potential for larger clusters is constructed from an accurate three body Rg–HX term (for $HI(Ar)_n$ we have used Bevan's semiempirical potential [5], for $HI(Ne)_n$ and $HBr(Ne)_n$ systems we have used the present *ab initio* potentials) and from pair potentials for Rg-Rg interactions [59]. The heavy atom geometries of the $HI(Ar)_n$, $HBr(Ne)_n$ and $HI(Ne)_n$ clusters are similar to those of $HCl(Ar)_n$ clusters [60]. Since the hydrogen halide is slightly too large to fit inside the cluster, it prefers the surface position even for large rare gas clusters. The symmetries of optimal structures, as obtained by potential minimization, are C_{2v} for HX(Ar)$_2$ system, C_{3v} for HX(Ar)$_3$, C_{2v} for HX(Ar)$_4$, C_{4v} for HX(Ar)$_5$ and C_{5v} for HX(Ar)$_6$.

The librational wavefunctions for HBr(Ne)$_n$ clusters are depicted in Fig. 7. The character of the ground librational state does not change dramatically upon increasing cluster size for the HBr(Ne)$_n$ and HI(Ne)$_n$ clusters. Starting from a single rare gas solvent atom, the hydrogen wavefunction is pointing towards the cluster. Therefore, after photodissociation, one can expect a significant cage effect, and consequently, the shift to smaller values in the kinetic energy distribution of the H fragment.

The situation for HI(Ar)$_n$ clusters is more complicated and interesting at the same time. The hydrogen wavefunctions for this complex are depicted in Fig. 8. The ground state of the smallest cluster with a single rare gas atom is associated with the Ar–IH geometry. Also in the HI(Ar)$_2$ complex hydrogen points away from the rare gas atoms. The crucial point is, that for HI(Ar)$_3$ the librational wavefunction flips and the hydrogen now points towards the argons. For HI(Ar)$_4$ hydrogen flips back and the situation is similar to HI(Ar)$_2$, since HI interacts effectively only with the two closer argon atoms. Starting from the HI(Ar)$_5$ cluster the optimal vibrationally averaged structure corresponds again to the IH–Rg$_n$ geometry. In conclusion, although hydrogen points away from the complex for the HI(Ar)$_n$ (n=1,2,and 4) clusters, starting from five argons surface solvated HI always has hydrogen pointing towards the rare gas atoms.

There is a nice piece of experimental evidence supporting the present calculated size evolution of the hydrogen wavefunction in HI(Ar)$_n$ clusters based on comparison of the measurements of Wittig et al. [36] and the experiments of Baumfalk and Buck [31,32]. Wittig reported the photodissociation of Ar$\cdots$HI complex, where no caging was detected (the H kinetic energy distribution was actually shifted to slightly higher energies), while Baumfalk and Buck studied large argon clusters (approximately 100 argon atoms) with HI on the surface and significant caging was observed. In future, it would be interesting to explore the predicted flip of the the hydrogen wavefunction in more detail. In particular, an experimental study of $HI(Ar)_2$ and $HI(Ar)_3$ should bring new insight into the intriguing quantum behavior of these systems.

V. CONCLUSIONS

The main points addressed in the present paper can be summarized as follows:

1. We have calculated using the CCSD(T) *ab initio* method accurate potential energy surfaces of Ne···HBr and Ne···HI.

2. We have constructed intermolecular vibrational states of Ne···HBr, Ne···HI, and $HI(Ar)_n$ (n=1-6).

3. We have shown that for cryogenic complexes containing hydrogen moving in a shallow bending potential a correct description should be based on vibrationally averaged structures rather than on minima on the potential energy surfaces.

4. We have demonstrated that for the Ne···HI cluster the global minimum corresponds to the Ne–IH geometry, however, the optimal vibrationally averaged structure has hydrogen between the heavy atoms.

5. We have interpreted seemingly conflicting experimental data on HI···Ar and large $HI(Ar)_n$ clusters in terms of a flip of the hydrogen towards the rare gas atoms upon increasing the number of argons.

In summary, the main goal has been to demonstrate the importance of quantum delocalization, in particular that connected with the large amplitude hydrogen bending motion, in cryogenic Rg···HX clusters. As a matter of fact, the vibrational quantum effect can become more important for determining the energetically lowest isomeric structure than the relative depths of the minima on the PES.

Acknowledgment

We are grateful to R. R. Lucchese for providing us their Ar$\cdots$HI potential and to K. Faegri for sending us his basis set. This work has been supported by the Volkswagen foundation via the grant No. I/75908. Support of the Czech Ministry of Education to the Center for Complex Molecular Systems and Biomolecules (grant No. LN00A032) is gratefully acknowledged.

REFERENCES

[1] K. R. Leopold, G. T. Fraser, S. E. Novick, and W. Klemperer, Chem. Rev. **94**, 1807 (1994).

[2] R. L. Robinson, D.-H. Gwo, and R. J. Saykally, J. Chem. Phys. **87**, 5149 (1987).

[3] M. R. Keenan, E. J. Campbell, T. J. Balle, L. W. Buxton, T. K. Minton, P. D. Soper, and W. H. Flygare, J. Chem. Phys. **72**, 3070 (1980).

[4] D. W. Firth, M. A. Dvorak, S. W. Reeve, R. S. Ford, and K. R. Leopold, Chem. Phys. Lett. **168**, 161 (1990).

[5] A. McIntosh, Z. Wang, J. Castillo-Chará, R. R. Lucchese, J. W. Bevan, R. D. Suenram, and A. C. Legon, J. Chem. Phys. **111**, 5764 (1999).

[6] J. Han, A. L. McIntosh, Z. Wang, R. R. Lucchese and J. W. Bevan, Chem. Phys. Lett., **265**, 209 (1997).

[7] J. M. Hutson, J. Chem. Phys. **89**, 4550 (1988).

[8] J. M. Hutson, J. Phys. Chem. **96**, 4237 (1992).

[9] J. M. Hutson, J. Chem. Phys. **96**, 6752 (1992).

[10] M. Meuwly and J. M. Hutson, J. Chem. Phys. **110**, 8338 (1999).

[11] J. M. Hutson, J. Chem. Phys. **91** 4448 (1989).

[12] J. M. Hutson, J. Chem. Phys. **91**, 4455 (1989).

[13] P. Niyaz, Z. Bacic, J. W. Moskowitz, and K. E. Schmidt, Chem. Phys. Lett. **252**, 23 (1996).

[14] C. E. Dykstra, J. Chem. Phys. **108**, 6619 (1998).

[15] M. Lewerenz, J. Chem. Phys. **104**, 1028 (1996).

[16] J. Franck and E. Rabinowitch, Trans. Faraday Soc. **30**, 120 (1934).

[17] A. Garcia-Vela, J. Chem. Phys. **108**, 5755 (1998).

[18] T. Schroeder, R. Schinke, M. Mandziuk, and Z. Bacic, J. Chem. Phys. **100**, 7239 (1994).

[19] E. Narevicius, D. Neuhauser, H. J. Korsch, and N. Moiseyev, Chem. Phys. Lett. **276**, 250 (1997).

[20] M. Monnerville and B. Pouilly, Chem. Phys. Lett. **294**, 473 (1998).

[21] A. Garcia-Vela, R. B. Gerber, and U. Buck, J. Phys. Chem. **98**, 3518 (1994).

[22] R. Alimi and R. B. Gerber, Phys. Rev. Lett. **64**, 1453 (1990).

[23] M. Niv, A. I. Krylov, and R. B. Gerber, Faraday Discuss. Chem. Soc. **108**, 243 (1997).

[24] M. Niv, A. I. Krylov, R. B. Gerber, and U. Buck, J. Chem. Phys. **1110**, 11047 (1999).

[25] R. Baumfalk, N. H. Nahler, U. Buck, M. Y. Niv, and R. B. Gerber, J. Chem. Phys., **113**, 329 (2000).

[26] B. Schmidt, P. Jungwirth, and R. B. Gerber, in "Ultrafast Chemical and Physical Processes in Molecular Systems" (ed. M. Chergui) World Scientific, Singapore, 1996, p. 637.

[27] J. Manz, P. Saalfrank, and B. Schmidt, J. Chem. Soc. Faraday Trans. **93**, 957 (1997).

[28] B. Schmidt, Chem. Phys. Lett. **301**, 207 (1999).

[29] P. Zdanska, B. Schmidt, and P. Jungwirth, J. Chem. Phys. **110**, 6246 (1999).

[30] P. Zdanska, P. Slavicek, and P. Jungwirth, J. Chem. Phys., **112**, 10761 (2000).

[31] R. Baumfalk, Ph. D. Thesis, Göttingen 1999.

[32] R. Baumfalk and U. Buck, Faraday Disc. Chem. Soc., in press.

[33] T. A. Beu, U. Buck, I. Ettischer, M. Hobein, J. G. Siebers, and R. J. Wheatley, J.

Chem. Phys., **106**, 6806 (1997).

[34] D. C. Clary, D. M. Benoit, T. V. Mourik, Acc. Chem. Res. **33**, 441 (2000).

[35] K. Liu, M. G. Brown, C. Carter, R. J. Saykally, J. K. Gregory, and D. C. Clary, Nature **381**, 501 (1996).

[36] C. Jaques, L. Valachovic, S. Ionov, E. Böhmer, Y. Wen, J.Segall and C. Wittig, J. Chem. Soc. Faraday Trans., **89**, 1419 (1993).

[37] S. F. Boys and F. Bernandi, Mol. Phys. **19**, 553 (1970).

[38] http://www.emsl.pnl.gov:2080/forms/basisform.html

[39] D. E. Woon and T. H. Dunning, Jr., J. Chem. Phys. **98**, 1358 (1993).

[40] A. K. Wilson, D. E. Woon, K. A. Peterson, and T. H. Dunning, Jr., J. Chem. Phys. **110**, 7667 (1999).

[41] T.H. Dunning, Jr., J. Chem. Phys. **90**, 1007 (1989).

[42] P.O. Widmark, B. J. Persson, and B. Roos, Theor. Chim. Acta, **79**,419 (1991).

[43] G. Chałasiński, M. M. Szczęśniak and B. Kukawska-Tarnawska, J. Chem. Phys. **94**, 6677(1991).

[44] L.A. LaJohn, P. A. Christiansen, R. B. Ross, T. Atashroo, and W. C. Ermler, J. Chem. Phys. **87**, 2812(1987).

[45] L. Visscher and K. G. Dyall, J. Chem. Phys. **104**, 9040(1996).

[46] L. Visscher, J. Styszyñski, and W. C. Nieuwpoort, J. Chem. Phys. **105**, 1987(1996), K. Faegri, private communication.

[47] J. V. Burda, P. Hobza and R. Zahradník, Chem. Phys. Lett. **288**, 20 (1998).

[48] F.-M. Tao and Y.-K. Pan, Chem. Phys. Lett. **194**, 162 (1992); J. Chem. Phys. **97**, 4989

(1992).

[49] F.-M. Tao and W. Klemperer, J. Chem. Phys. **101**, 1129 (1994).

[50] R. Burcl, G. Chałasiński, R. Bukowski, and M. M. Szczęśniak, J. Chem. Phys. **103**, 1498 (1995).

[51] H. L. Williams, E. M. Mas, K. Szalewicz and B. Jeziorksi, J. Chem. Phys. **103**, 7374 (1995).

[52] Gaussian98; M. J. Frisch, G. W. Trucks, H. B. Schlegel, G. E. Scuseria, M. A. Robb, J. R. Cheeseman, V. G. Zakrzewski, J. A. Montgomery, R. E. Stratmann, J. C. Burant, S. Dapprich, J. M. Millam, A. D. Daniels, K. N. Kudin, M. C Strain, O. Farkas, J. Tomasi, V. Barone, M. Cossi, R. Cammi, B. Mennucci, C. Pomelli, C. Adamo, S. Clifford, J. Ochterski, G. A. Petersson, P. Y. Ayala, Q. Cui, K. Morokuma, D. K. Malick, A. D. Rabuck, K. Raghavachari, J. B. Foresman, J. Cioslowski, J. V. Ortiz, B. B. Stefanov, G. Liu, A. Liashenko, P. Piskorz, I. Komaromi, R. Gomperts, R. L. Martin, D. J. Fox, T. Keith, M. A. Al-Laham, C. Y. Peng, A. Nanayakkara, C. Gonzales, M. Challacombe, P. M. W. Gill, B. G. Johnson, W. Chen, M. W. Wong, J. L. Andres, M. Head-Gordon, E. S. Reploge and J. A. Pople, Gaussian Inc.: Pittsburgh, PA, 1998.

[53] R. Kosloff and H. Tal-Ezer, Chem. Phys. Lett., **127**, 223 (1986).

[54] T. Suzuki, H. Katayanagi, and M. C. Heaven, J. Phys. Chem. **101**, 6697(1997).

[55] A. Bagno, J. Chem. Soc., Faraday Trans. **94**, 2501(1998).

[56] G. Herzberg, Molecular spectra and molecular structure, Van Nostrand, New York, 1950.

[57] R. Kosloff, J. Phys. Chem. **92**, 2087 (1988).

[58] P. Slavicek, P. Zdanska, P. Jungwirth, R. Baumfalk and U. Buck, J. Phys. Chem. A **104**, 7793 (2000).

[59] R. A. Aziz and M. J. Slaman, Mol. Phys. **58**, 679 (1986).

[60] D. T. Anderson, S. Davis, and D. J. Nesbitt, J. Chem. Phys. **107** , 1115 (1997).

TABLE CAPTIONS

Table 1: Basis sets and contraction schemes used in the *ab initio* calculations.

Table 2: Results of test calculations at the CCSD(T) level. The table compares the global and secondary minima of the PES for four different Rg$\cdots$HX complexes with the results of previous studies.

Table 3: Results of calculations at the CCSD(T) level for the global and secondary minima, as well as the barrier (saddle) separating them, for Ne$\cdots$HBr and Ne$\cdots$HI complexes.

Table 4: Energies of the lowest bound intermolecular vibrational states of Ne$\cdots$HBr and Ne$\cdots$HI complexes in cm^{-1}.

Table 5: Summary of the three prototypical cases of Rg$\cdots$HX complexes. The table compares energies and structures of minima on the PES with vibrationally averaged structures.

FIGURE CAPTIONS

Figure 1: Geometry and Jacobi coordinates (r, R, Θ) of the Rg$\cdots$HX complex. The filled circle half way between the Rg–X and Rg–H midpoints indicates the position of the bond functions used in the *ab initio* calculations.

Figure 2: Potential energy surface of the Ne$\cdots$HBr complex in the (R, Θ) plane obtained by CCSD(T) calculations. The contour labels give the interaction energy in cm^{-1}. Note that a value of $\Theta = 0^0$ corresponds to the Ne–HBr geometry, while $\Theta = 180^o$ corresponds to the Ne–BrH arrangement.

Figure 3: Same as Figure 2 but for the Ne$\cdots$HI complex.

Figure 4: Vibrational densities (squared moduli of the wavefunctions) for the Ne$\cdots$HI complex corresponding to a Ne–HI vibrationally averaged structure (Σ^+ symmetry). a) Vibrational ground state ($\epsilon = -28.3$ cm^{-1}). b) Second vibrationally excited state ($\epsilon = -16.1$ cm^{-1}). Full line coresponds to positive and dashed line to negative sign of the corresponding vibrational wavefunction.

Figure 5: Vibrational densities (squared moduli of the wavefunctions) for the Ne$\cdots$HI complex corresponding to a Ne–IH vibrationally averaged structure (Σ^+ symmetry). a) First vibrationally excited state ($\epsilon = -19.4$ cm^{-1}). b) Fourth vibrationally excited state ($\epsilon = -9.7$ cm^{-1}). Full line coresponds to positive and dashed line to negative sign of the corresponding vibrational wavefunction.

Figure 6: Vibrational densities (squared moduli of the wavefunctions) for the Ne$\cdots$HI complex corresponding to a T–shaped vibrationally averaged structure (Π symmetry). a) Third vibrationally excited state ($\epsilon = -12.4$ cm^{-1}). b) Fifth vibrationally excited state ($\epsilon = -2.3$ cm^{-1}). Full line coresponds to positive and dashed line to negative sign of the corresponding vibrational wavefunction.

Figure 7: Size dependence of the ground vibrational (librational) wavefunction for HBr on Ne$_n$ ($n = 1 - -6$). Note that in all cases the hydrogen atom points towards the rare gas clusters.

Figure 8: Size dependence of the ground vibrational (librational) wavefunction for HI on Ar_n ($n = 1 - -6$). Note the flip of the H wavefunction towards the rare gas clusters upon increasing cluster size.

Table 1, Slavicek et al.:

location	basis set
H	(5s2p1d)/[3s2p]
Cl	(13s9p2d1f)/[5s4p2d1f]
Br	(15s12p7d1f)/[16s5p3d]
I	AREP + (7s5p4d1f)
Ne	(14s9p4d)/[4s3p2d]
Ar	(13s9p2d1f)/[5s4p2d1f]
midbond region	3s(0.9,0.3,0.1),3p(0.9,0.3,0.1),2d(0.6,0.2)

Table 2, Slavicek et al.:

system	$\Theta/^o$	CCSD(T) calculation / cm^{-1}	MP2 calculation / cm^{-1}	previous value/cm^{-1}	reference
Ar..HCl	0	–173	–191	–175	[7]
Ar..HCl	180	–141	–161	–139	[7]
Ar..HBr	0	–168	–190	–165	[12]
Ar..HBr	180	–158	–181	–160	[12]
Ne..HCl	0	–66	–59	–68	[8]
Ne..HCl	180	–52	–48	–53	[8]
Ar..HI	180	–185	–215	–220	[5]
Ar..HI	0	–148	–174	–173	[5]

Table 3, Slavicek et al.:

	Ne$\cdots$HBr	Ne$\cdots$HI
$\epsilon(0^o)/\mathrm{cm}^{-1}$	-58.6	-48.1
$\epsilon(90^o)/\mathrm{cm}^{-1}$	-30.5	-28.5
$\epsilon(180^o)/\mathrm{cm}^{-1}$	-55.7	-55.7
$R_m(0^o)/\text{Å}$	4.07	4.48
$R_m(90^o)/\text{Å}$	4.00	4.30
$R_m(180^o)/\text{Å}$	3.55	3.75

Table 4, Slavicek et al.:

Symmetry	Ne$\cdots$HBr	Ne$\cdots$HI
Σ^+	–29.0	–28.3
Σ^+	–15.6	–19.4
Σ^+	–12.9	–16.1
Σ^+	–5.4	–9.7
Π	–8.4	–12.4
Π		–2.3

Table 5, Slavicek et al.:

system	minimum on PES	D_e / cm^{-1}	structure	D_0 / cm^{-1}
Ne$\cdots$HBr	Ne–HBr	–58.6	Ne–HBr	–29.0
Ar$\cdots$HI [5]	Ar–IH	–220.0	Ar–IH	–146.4
Ne$\cdots$HI	Ne–IH	–55.7	Ne–HI	–28.3

Figure 1, Slavicek et al.:

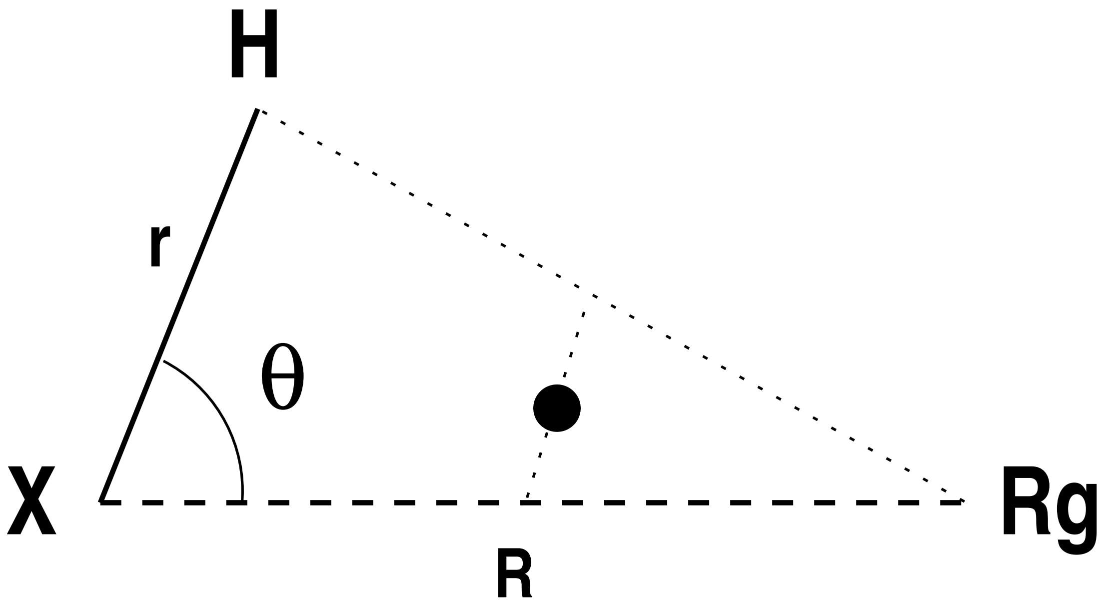

Figure 2, Slavicek et al.:

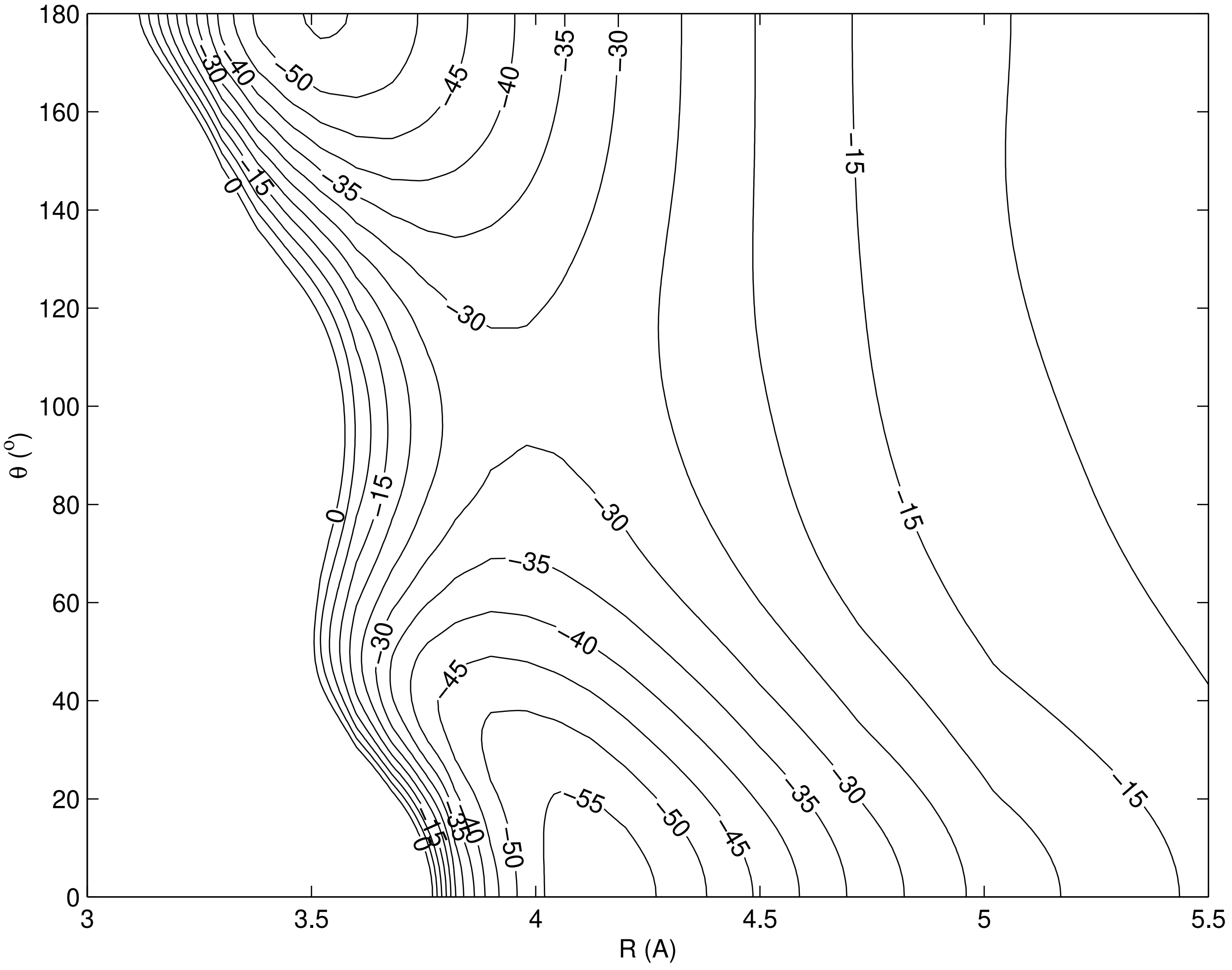

Figure 3, Slavicek et al.:

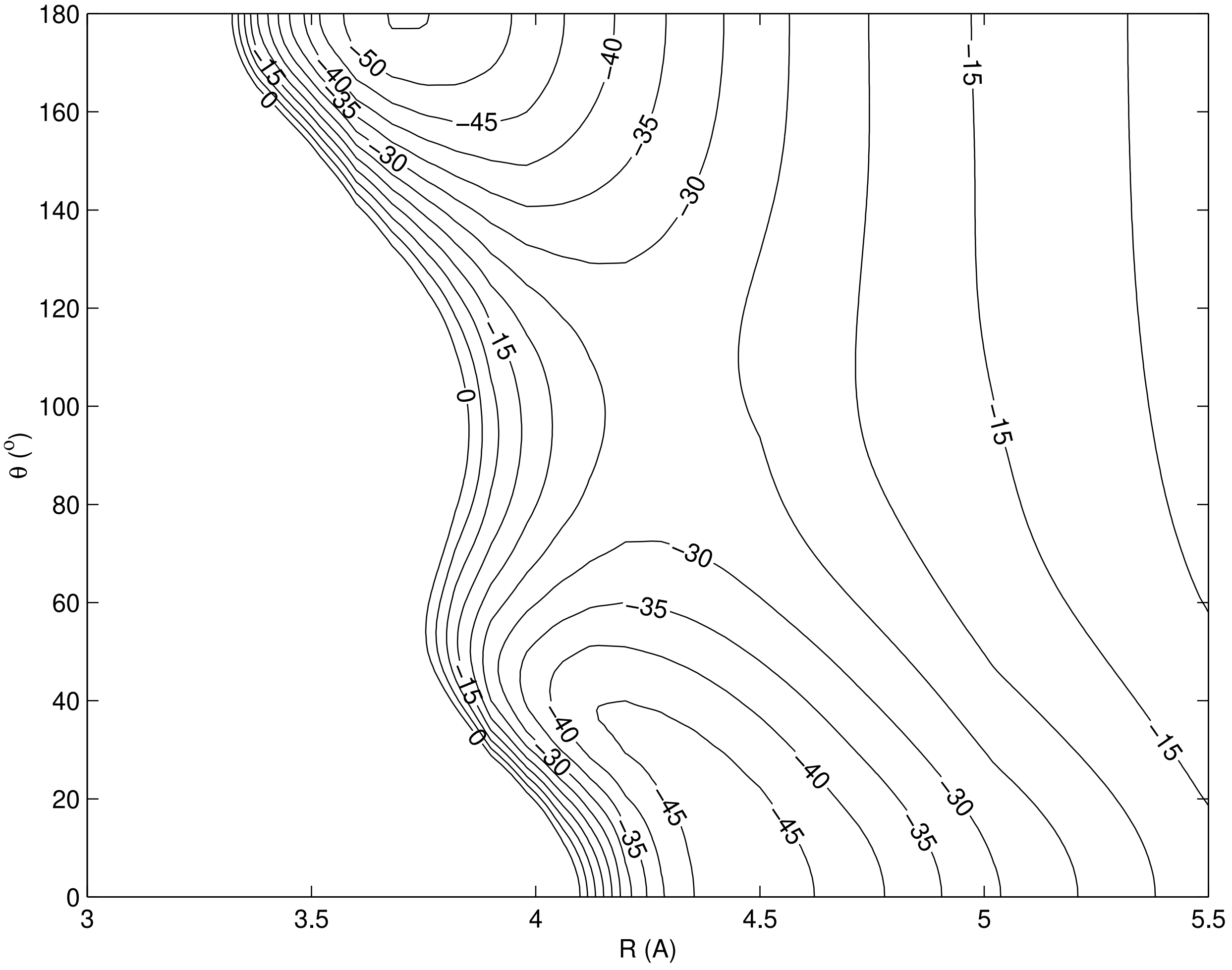

Figure 4, Slavicek et al.:

a)

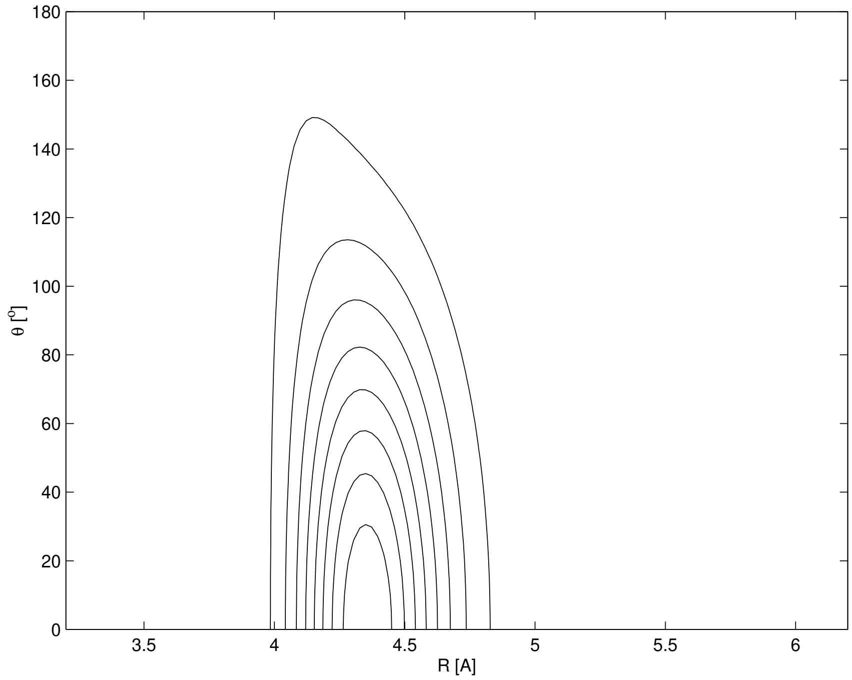

b)

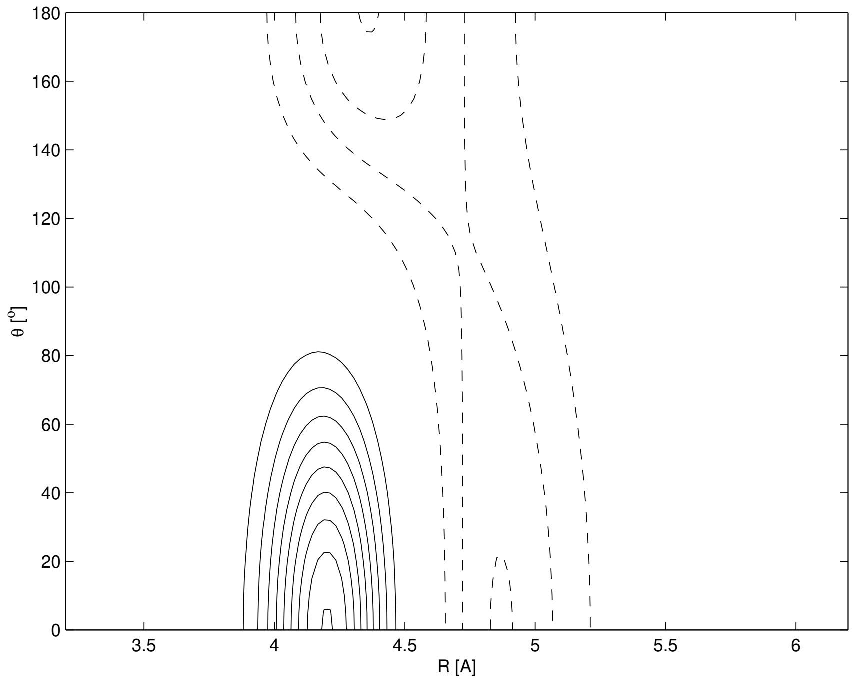

Figure 5, Slavicek et al.:

a)

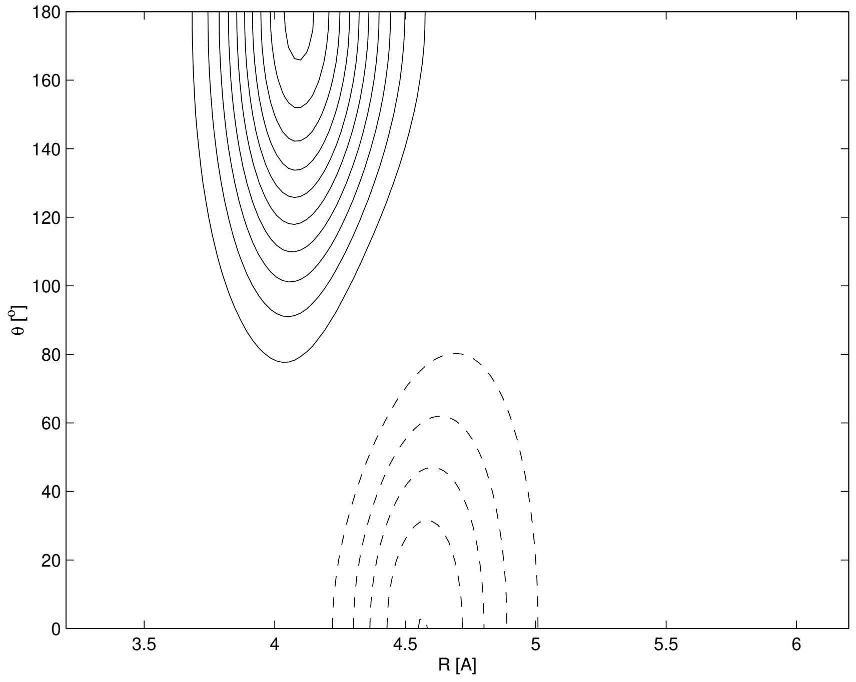

b)

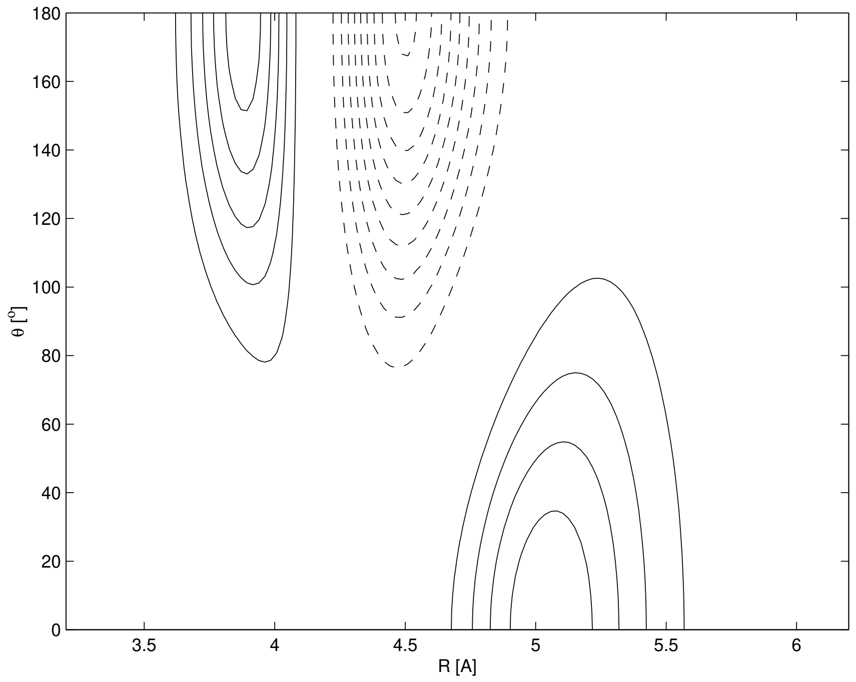

Figure 6, Slavicek et al.:

a)

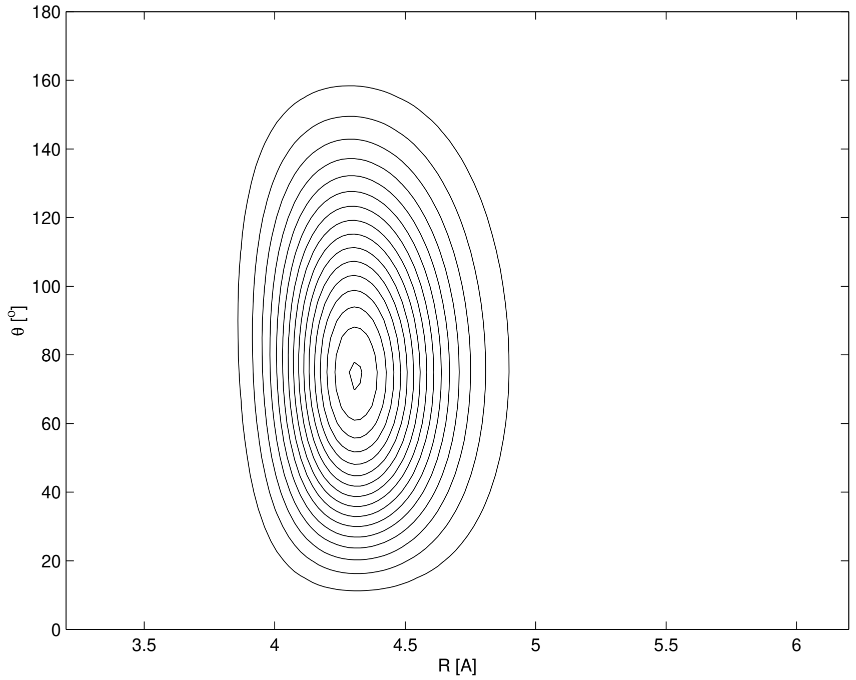

b)

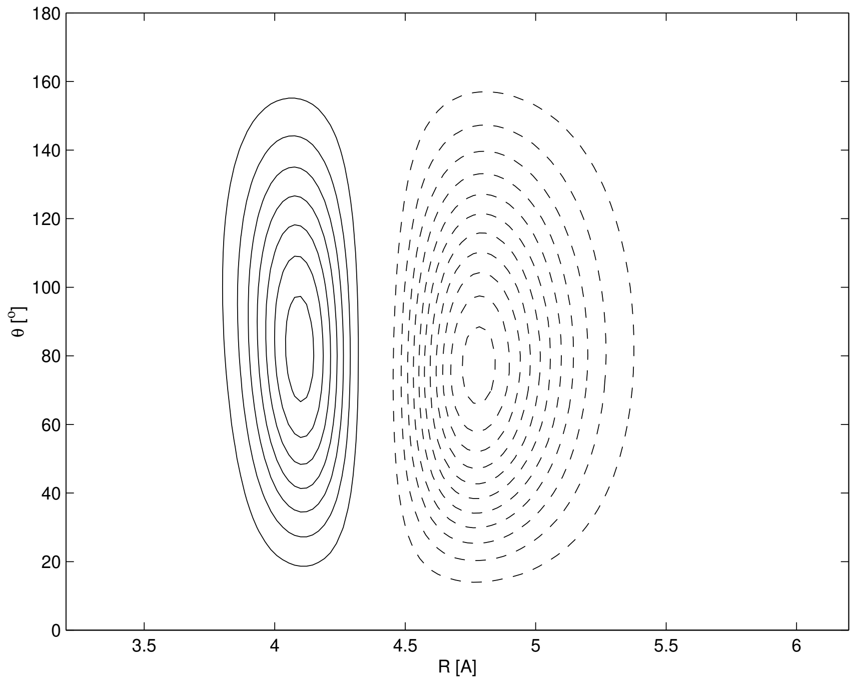

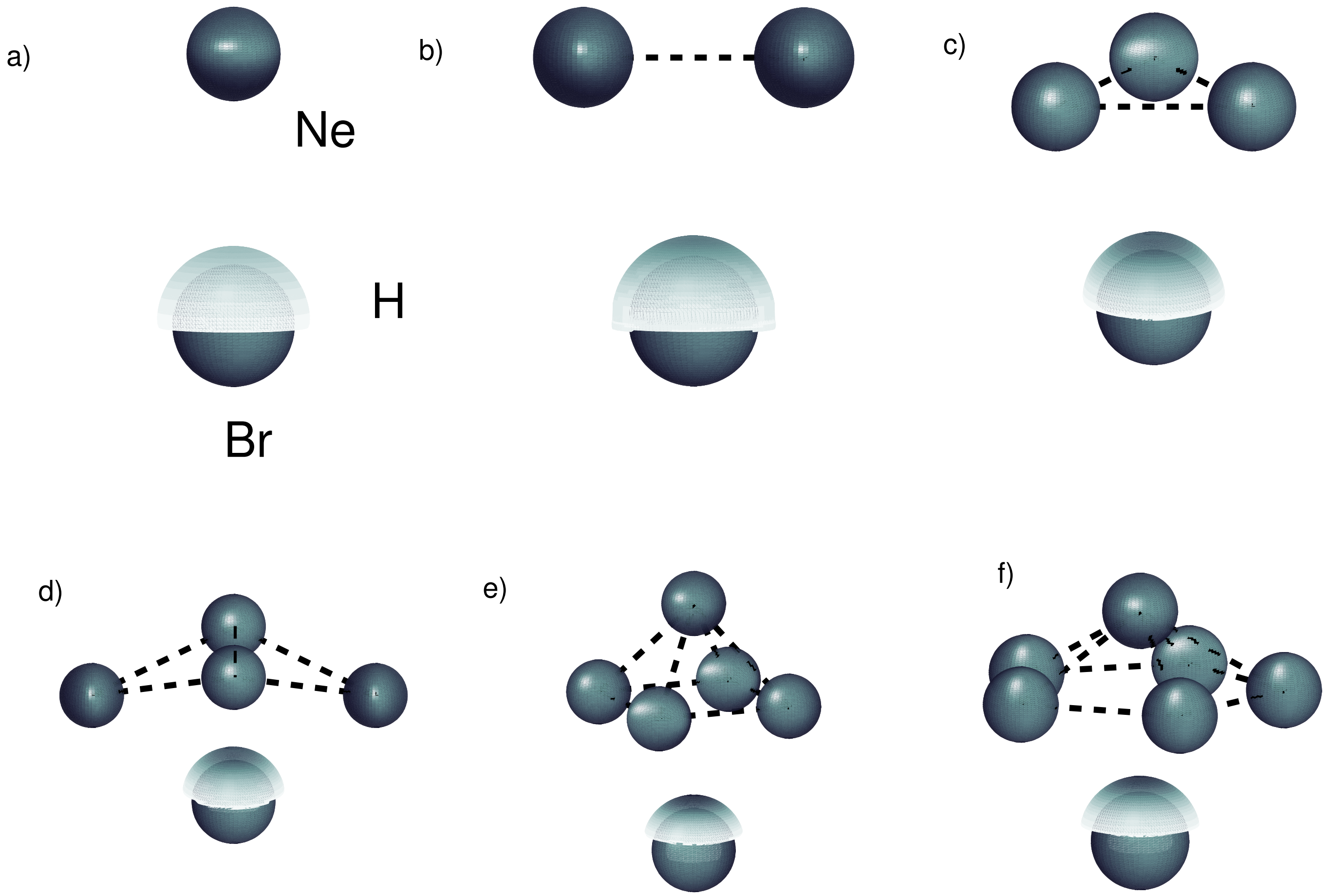

Figure 7, Slavicek et al.:

Figure 8, Slavicek et al.: